Equivalent strain distribution at high pressure torsion extrusion of pure copper: Finite element modeling and experimental validation

Dayan Nugmanov [a,*], Roman Kulagin [a], Olivier Perroud [b], Matthias Mail [c], Horst Hahn [a], Yulia Ivanisenko [a]

[a] Institute of Nanotechnology (INT), Karlsruhe Institute of Technology (KIT), 76021 Karlsruhe, Germany
[b] Laboratory of Microstructures and Materials Mechanics (LEM 3), UMR 7239, CNRS/University of Lorraine, F-57045 Metz, France
[c] Karlsruhe Nano Micro Facility, Karlsruhe Institute of Technology, Eggenstein-Leopoldshafen 76344, Germany

ARTICLE INFO

Keywords:
Finite element modeling
Strain distribution
High pressure torsion extrusion
X-ray tomography
Severe plastic deformation

ABSTRACT

Results of finite element modeling of strain state of the sample were experimentally validated using copper samples with aluminum markers and analyzed for a deep understanding of the influence of processing parameters and materials properties on the strain distribution in the billets processed by high pressure torsion extrusion (HPTE). Calculations were carried out for pure copper for HPTE regimes with resulting strain in a range between 0.9 and 12.0 at deformation temperatures of 25 and 100 °C. It was established that the accumulated strain in HPTE can be as high as ~1.5 even at the axis of the sample, which shows the high efficiency of HPTE as a method of severe plastic deformation. A comparison of the calculated strain distributions with experimentally measured ones in copper billets made it possible to reveal the spreading of the deformation zone along the height of the sample, caused by its slippage in the die. It was established that this slippage increases with increasing of deformation temperature and with the value of accumulated strain. X-ray tomography was used to visualize the change of the shape of wire markers inserted in the samples prior to HPTE processing.

1. Introduction

Severe plastic deformation (SPD) methods are especially attractive because they open up new opportunities for the production of bulk nanostructured materials (BNM) at industrial scale and allow the creation of ultrafine grained (UFG) structures at various length scales (Valiev et al., 2000). High pressure torsion (HPT) is the most effective (in respect of microstructure refinement) method of SPD, however the size of processed samples is limited to a size of a coin. Several attempts were undertaken to scale up the HPT method (Pippan et al., 2008). The experience of using deformation methods that implement a direct extrusion in combination with torsion, such as incremental high pressure torsion (Pippan et al., 2008), torsion extrusion using a square-hole die (Mizunuma et al., 2010) high pressure tube twisting (Toth et al., 2019) and several other methods show that all these methods have one main problem related to insufficient friction at the surface of the billet. To overcome this problem, a new method, scaling up the conventional HPT process, High Pressure Torsion Extrusion (HPTE), has been presented by Ivanisenko et al. (Fedorov et al., 2015). HPTE was not the first attempt to combine torsion deformation with extrusion. As have recently shown by Pardis et al. (2011), the idea of the accumulation of severe deformation according to the simple shear conditions was borrowed from HPT, while the expansion - extrusion die sections provide the necessary back pressure in the deformation zone, similar as in cyclic expansion extrusion.

Finite element method (FEM) modelling allows to visualize the stress and strain distribution in the work piece, which is very useful for understanding, developing and optimizing metal-forming processes. FEM was successfully used for modelling of ECAP (Baik et al., 2003), twist extrusion (Beygelzimer et al., 2006) and some other methods of severe plastic deformation. There were also attempts to use it for HPTE (Ivanisenko et al., 2016). Unfortunately FEM modelling of HPTE process is not a trivial task, due to the following reasons. One would assume that the motion of the deforming tool is fully transmitted to the billet. However, this might be not the case due to a possible slippage of the billet within the rotating die (Kulagin et al., 2019). In the work (Kulagin et al., 2013) it was shown that neither the appearance of the stress-strain curve, nor the variation of friction coefficients allowed to fit the FEM

* Corresponding author.
E-mail address: dayan.nugmanov@kit.edu (D. Nugmanov).

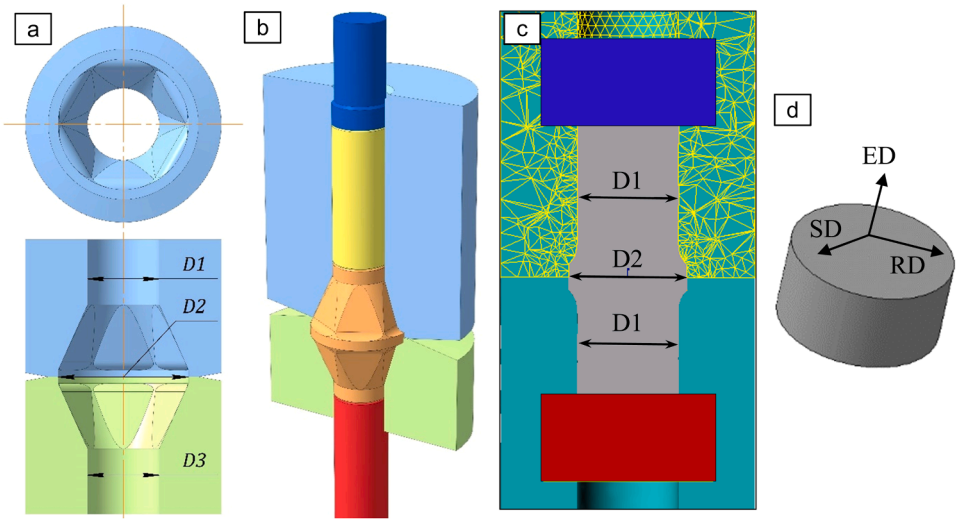

Fig. 1. Schematic drawing of the HPTE tool (a) and 3D image of three experimentally used billets inside the HPTE die (processing billets are marked by the yellow, orange and red colors) (b). Set of tools and billet for the FEM: diametric section of the assembled punch (blue rectangle), plug red rectangle), top HPTE die (cyan shape covered by the meshing lines network), bottom line (cyan shape) and billet (grey) (c). External directions are shown as radial direction (RD), extrusion direction (ED) and shear direction (SD) (d).

model so that it fully reproduced the experiment. The explanation for this effect was that the FEM model exploits the von Mises isotropic plasticity model, which does not allow to take into account the deformation scheme. The stress-strain state of the billet at HPTE comprises both simple shear (torsion) and pure shear (expansion and extrusion). As the final shape of the billet does not change as a result of processing, it is impossible to conclude about the real strain experienced by the billet. In the present work we used a marker-insert technique to precisely examine the metal flow in HPTE at different strain regimes and at two different temperatures. The as-obtained information was used to adjust FEM simulations, and allowed to describe the real strain distribution in the copper billet. The proposed approach can be useful for the analysis of metal-forming processes when the strain cannot be straightforwardly determined.

2. Principles of the HPTE process

Schematic drawing of HPTE dies is demonstrated in Fig. 1a. The conical shape of the hollow space (Fig. 1a, bottom) allows to create a required level of hydrostatic pressure in the shear zone. The theoretical equivalent strain 'e' accumulated in the sample as a function of the radius position R after one pass can be controlled as a function of the ratios of the sample diameters (D2/D1, where D1 = 12.0 mm, D2 = 14.0 mm), final diameter reduction for the back pressure (D1/D3, where D3 = 10.8 mm) and the processing translation/rotation velocities(v/ω) of the tools with smooth conical surfaces according to the equation (Ivanisenko et al., 2016):

$$e = 4\ln\frac{D2}{D1} + 2\ln\frac{D1}{D3} + \frac{\omega \bullet R}{\sqrt{3} \bullet v}\frac{D2}{D1} \quad (1)$$

In order to avoid slippage of the billet in the die, a hexagonal shape of the HPTE die channel was developed and applied (Ivanisenko et al., 2016). It has been experimentally demonstrated that such configuration of HPTE die (Fig. 1a) is perfect for the obtaining large strain in copper billets (Ivanisenko et al., 2016). In the present work, the cylindrical billets with an initial length of 35 mm and diameter of 11.8 mm were processed at room temperature and at 100 °C. Due to geometrical constraints related to the length of the punch in a real HPTE process, three billets needed to be used at the same time (Fig. 1b). Thanks to a tight junction between them, all three billets were deformed as a whole long bar.

The hexagon shape of the HPTE die (Fig. 1a, b) makes a precise calculation of the accumulated strain in the billet a very difficult task. In the following, the results of the analytical calculation of the strain for dies with a simple conical shape and also with hexagonal shape, for various HPTE regimes using the finite element method (FEM), will be presented.

3. Materials and methods

3.1. Samples preparation and experimental investigation methods

The metal flow during HPTE was analyzed by a marker-insert technique. Commercially pure aluminum wires were used as markers tracing a real material flow in commercially pure copper billets during the HPTE process.

A sufficiently good junction between wires and the matrix was obtained by direct extrusion of copper cylinder with embedded aluminum wires from the diameter of 20–11.8 mm, upon that the diameter of wires was reduced from 2.0 to 1.2 mm. Two sample configurations: (i) with six

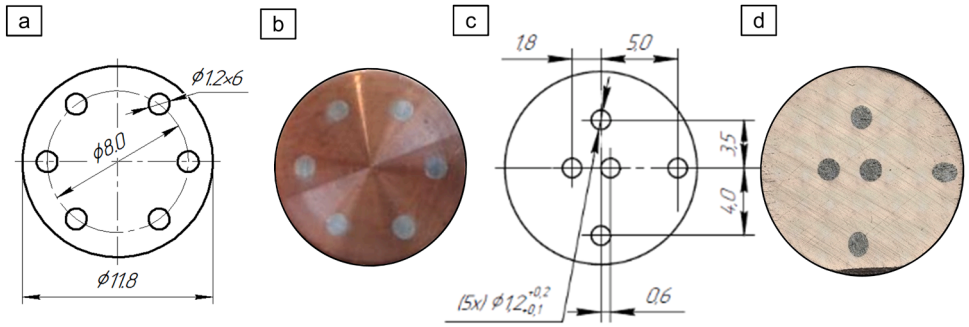

Fig. 2. Design of the initial billets with wires (a, c). Transversal sections of the copper samples with aluminum markers before HPTE. Figure b, d– optical microscope.

Table 1
Regimes of HPTE process and respective von Mises strain for cone-shape dies.

Process ID	v mm/min	ω rpm	strain		
			center	mid_rad	edge
$v10\omega0$*	10	0	0.9	0.9	0.9
$v6\omega1$	6	1	0.9	3.0	5.2

* v is the translation velocity and ω is the rotation velocity of the HPTE tool.

aluminum wires placed at a distance of 4.0 mm from the center of the rod (Fig. 2a, b) and with five wires, placed at different distances from the center of the copper billet (Fig. 2c, d), were subjected to HPTE, at 25 °C and at 100 °C.

Copper billets with a diameter of 11.8 mm (Fig. 2) and a height of 35 mm with inserted aluminum wires were processed by HPTE, using the $v10w0$ and $v6w1$ regimes. In case of the $v10\omega0$ HPTE regime, there is no bottom die rotation and during the $v6\omega1$ regime, bottom die was rotated 5.8 times during the entire length of the billet had passed through the shear plane.

In order to analyse the strain state in the billet directly in the deformation zone (in the following referred to as *intermediate processing),* the deformation process was stopped when half of the billet had passed. This situation is illustrated for the orange billet in this position in Fig. 1b. Then the HPTE die was disassembled. In order to track marker wire shape and location, the obtained samples, as well as samples after completed HPTE, were sectioned as follows. Billets were cut through the extrusion direction (ED in Fig. 1d), and the as-obtained surfaces were grinded and polished with subsequently reduced roughness of the polishing suspension to obtain mirror-like surface. Optical images of the as-prepared and processed samples surfaces were recorded using Keyence VH-Z100R fixed in VHX-550 system microscope. SEM Zeiss LEO1530 operating at 20 kV and equipped with secondary electrons (SE) detector was used for the microstructure investigations.

Other billets with Al marker wires were fully processed by HPTE (in the following referred as *full-height processing)* and the resulting configuration was analyzed.

For a full-size non-destructive characterization of the 3D geometry of the hybrid samples after HPTE, X-Ray tomography measurements were performed. The setup is mounted on an X-ray computer tomography (CT) scanner Easytom Nano model provided by RX-Solutions, equipped with 160 kV micro-focus X-ray tube, with spatial resolution down to 0.35 μm. 3000 images along Y direction were obtained to build a 3D computed object using the Radon transform. The resulting 2D slices of the longitudinal sections were reconstructed to 3D images and were segmented using Dragonfly object recognition system (non-commercial edition).

3.2. Calculation of von Mises strain in HPTE process using the analytic equation and FEM simulations

Results of the von Mises strain calculation by Equation (1) at three points located in the sample cross section at different distances from the center for *cone-shape dies* in HPTE deformation are presented in Table 1.

Previous FEM simulations of the HPTE process (Ivanisenko et al., 2016) revealed that strains, calculated using Equation (1), very roughly represent the strain distribution in a real deformation process, because of the actual hexagonal shape of the dies (Fig. 1a). Also the friction conditions as well as the rheology of the material and the deformation history are not taken into account.

To clarify the strain distribution in the HPTE process with *hexagonal dies* (Fig. 1a) 3D finite element analyses were performed using the commercially available QForm VX 8.2.4 software, that has been described by Biba et al. (2012).

To simplify the calculations, FEM was performed for the middle billet

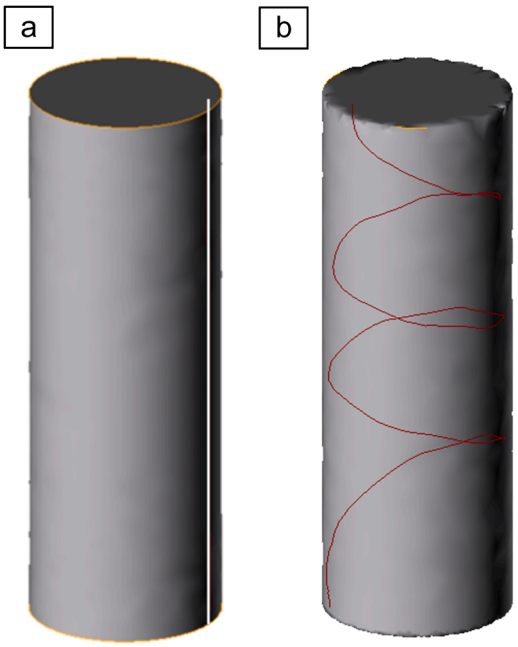

Fig. 3. 3D images of the billet and marker lines, used for the FEM, before (a) and after processing (b).

Table 2
Regimes of HPTE process and respective von Mises strain for cone-shape dies.

Parameter	Value
Density, kg/m3	8850
Thermal conductivity, W/(m*K)	385
Specific heat, J/(kg K)	390
Levanov coefficient	1.25
Young modulus, GPa	125
Poisson coefficient	0.35

(marked with orange color in Fig. 1b). The top and the bottom billets in the real HPTE process were replaced by the punch and plug tools in the simulation (marked by blue and red rectangles in Fig. 1c). Also for the simplicity reasons, D3 was chosen to be equal to D1.

3D image of the initial billet is shown in Fig. 3a. For the FEM analysis the marker line was placed parallel to the ED at a distance of 5 mm from the billet axis (marked by the white line in Fig. 3a). The marker line after the HPTE processing is shown by the red line in Fig. 3b. During the HPTE process, the billet was deformed using the regimes given in Table 1.

A 3D deformation problem with thermal processes was set for the strain-stress calculation.

Table 2 lists the material parameters for all simulations performed in this study. Levanov friction model was adopted (Levanov, 1997). According to the this model Levanov, 1997 shear stress on the contacting surface of a sample depends on the friction factor (m), flow stress (σ_f) of the billet material, normal contact pressure (σ_n), and Levanov coefficient (n, assumed to be equal to 1.25):

$$\tau = m\frac{\sigma_f}{\sqrt{3}}\left(1 \quad e^{-n\frac{\sigma_n}{\sigma_f}}\right)$$

Friction coefficients were chosen according to a procedure explained in Section 5.1. All FEM results were obtained in the steady state.

Due to the large strains reached during HPTE, the geometry of meshing elements is reconstructed every few calculation steps. The maximum number of calculation steps without remeshing was 20, the maximum external angle of the meshing element was - 151°. When the value of the external angle of the triangle exceeded 151°, the remeshing

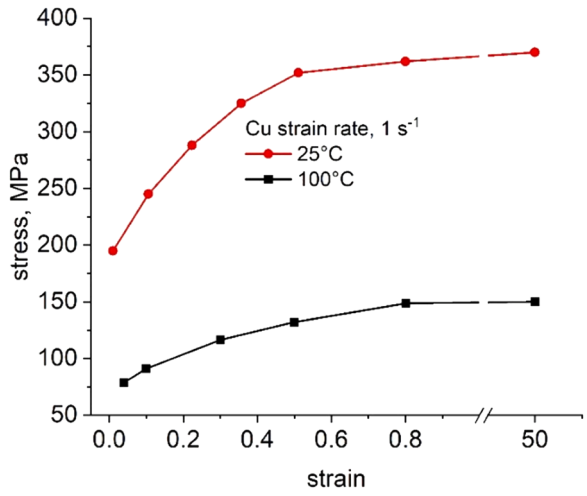

Fig. 4. Engineering stress-strain curves for FEM calculation of HPTE deformation of copper.

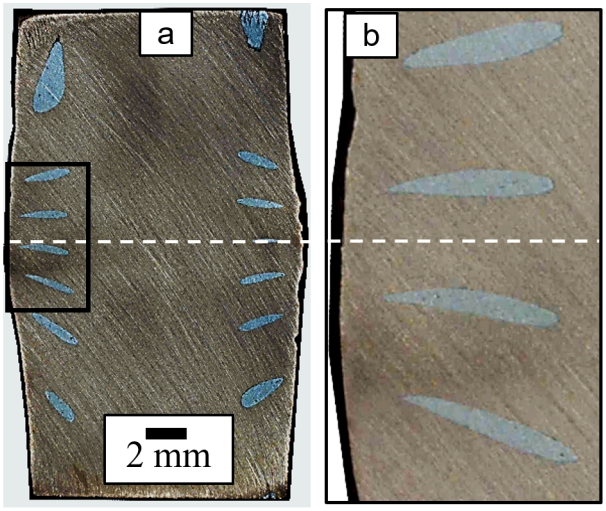

Fig. 5. Optical image of the longitudinal cross sections of the copper billets with six aluminum markers. Billet was processed by the *v*6*w*1 HPTE regime at 25 °C (b). ŧThe enlarged image of the area in a black frame in (a) is shown in (b).

procedure was initialized.

Strain hardening of each meshing element was calculated using the strain hardening curves of pure Cu shown in Fig. 4 from the QForm software database. Generally, for the examined HPTE regimes listed in the Table 1, the strain rates were ~ 1.0 s^{-1}.

4. Analysis of the strain state during HPTE

4.1. Intermediate processing

Fig. 5 illustrates how the aluminum wire markers, initially parallel to the ED, changed their shape during HPTE deformation. In Fig. 5 we can see that the wires obtained a helical shape after the *v*6*w*1 HPTE regime.

Longitudinal section of the billet demonstrated that the initial round shape of the wire transformed into a thin ribbon with the maximal narrowing at the bottom part of the billet. Note that the wires appeared to be severely deformed at a distance of 4–6 mm from the contact plane of the upper and lower HPTE dies (shown with the white dashed line in Fig. 5a), which approximately delineates the size of the shear deformation zone in HPTE. The drop-like shape of the cross section of the ribbon had maximal narrowing in the side, closest to the surface of a rod (Fig. 5b).

4.2. Full-height processing

Fig. 6 displays 2D images of the HPTE-processed sample after the *v*6*w*1 regime at 100 °C and 25 °C obtained by optical microscopy and X-ray tomography. In the latter case aluminum wires were identified as regions of interest (ROIs), highlighted in Fig. 6 by different colors.

Each wire was resolved as a separate ROI, that allowed to extract it from the conglomerate of six wires and to consider separately (Fig. 6a). As it was mentioned above for intermediate processing, the marker wires were transformed into ribbons.

The ribbons were inclined to the billet axis (Fig. 6a). This tilting appeared due to strong friction between the billet and the die-wall and typical for extrusion flow distortion (Holm et al., 2003). Each of the six wires was twisted for the equal number of loops $N_H = 1.4$ (Fig. 6a). N_H value was counted as a number of exit points of the marker wire on the longitudinal billet cross section. The loops of marker wire helixes were situated closer to each other at the bottom part of the billet as compared with their spatial distribution in the middle, and in the upper parts (Fig. 6a), which points towards the presence of stronger friction in the bottom die.

Transversal cross sections of the HPTE-processed billet demonstrate that the Al markers changed their shape from near-circular (Fig. 2b) to the drop-like one (Fig. 6c, d).

The degree of elongation of these “drops” is changing along the height of the sample: from slightly elongated “drops” in the top part of the bar (Fig. 6b) to much strongly elongated ones in the middle (Fig. 6c) and bottom parts (Fig. 6d).

The twisting of the marker wires is accompanied by the flow distortion typical for extrusion deformation. The effect of twisting by free end torsion is described in Grewe and Kappler (1964), whereas flow distortion typical for conventional direct extrusion is illustrated in Holm et al. (2003). These two flows lead to the change of marker wires shape from a circle to a teardrop in the cross-section perpendicular to the HPTE axis.

A similar approach to analyze the accumulated strain of the sample after the friction stir extrusion process is considered in Li et al. (2022). In this work, the markers were also introduced for the strain analysis. It was proposed to calculate radial strain and circumferential strain according to narrowing and extension of the marker in the cross section of the sample. Further research in this direction is necessary to obtain simple and reliable equations allowing to correctly calculate the equivalent strain of the sample in such complex processes.

Marker wires in the billet deformed at 25 °C (Fig. 6e) were twisted much stronger, than those in the sample deformed at 100 °C. Independently on the distance between the wire axis and the billet axis, all wires had equal number of loops $N_H = 3$, but the shapes of the wires cross sections were different (Fig. 6f-h). The wire placed close to the billet axis, retained its initial nearly-circular shape, while other wires changed their shape to ribbons. The same number of loops of the wires, placed at different distances from the billet axis in samples processed by *v*6*w*1 at 25 °C (Fig. 6e) demonstrates that all points in any transversal plane of a billet were rotated with the same angular velocity ω, as observed in Kulagin et al. (2019).

X-ray tomography allowed to count the number of loops of the marker wires in the billet after the HPTE *v*6ω1 regime (Table 3). After the *v*6ω1 regime, each wire was twisted for $N_H =$ at 25 °C and 1.4 at 100 °C while the number of the HPTE tool rotations was 5.8. Therefore the "experimental" rotation velocity w_e during HPTE processing was $w_e = 0.51$ and 0.24 for the *v*6ω1 regime at 25 and 100 °C, respectively. The reduced number of the marker wire loops in comparison with the number of the HPTE tool rotations indicates that there is significant slippage between the die walls and the billet, despite the presence of hexagon holding elements in the die design (Fig. 1a).

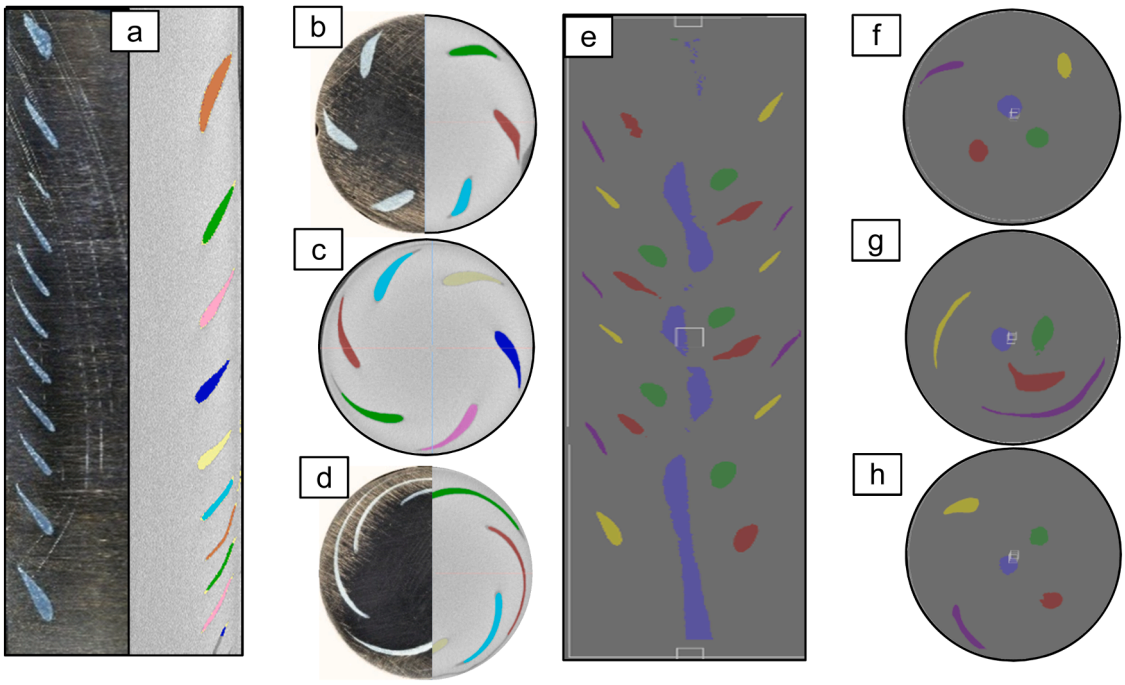

Fig. 6. 2D images of the aluminum wires in copper billets after HPTE *v*6*w*1 at 100 °C (a–d) and at 25 °C (e–h) in longitudinal (a, e) and transversal (b–d, f–h) sections for initial configurations with six (a–d) and five (e–h) wires. Optical microscopy is combined with results of X-ray tomography in (a, b, d).

Table 3
Experimentally obtained number of loops of the marker wires after HPTE process and values of friction coefficients employed for the FEM calculation.

T, °C	Process ID	N_H *	ω_e, rpm	Friction coefficient *m*			
				plug	punch	top die	bottom die
100 °C	*v*10*ω*0	0	0	0.1	0.1	0.6	0.6
	*v*6*ω*1	1.4	0.24	0.1	0.1	0.15	0.6
25 °C	*v*10*ω*0	0	0	0.1	0.1	0.6	0.6
	*v*6*ω*1	3.0	0.51	0.1	0.1	0.2	0.6

* N_H – number of loops of the embedded wire in full-height copper billet, experimentally measured after HPTE processing.

Summarizing the observations of the marker wires deformation resulting from different HPTE regimes, we can conclude that:

1. The size of the shear deformation zone in HPTE spreads for 4–6 mm from the contact plane of the upper and the lower HPTE dies.
2. In addition to shear (twisting) and expansion-extrusion deformation, there is a strong shearing in the periphery area of the billet due to friction and flow distortion typical for extrusion deformation.
3. There is a mismatch between the number of marker wire loops and the number of HPTE tool rotations, which indicates that there is significant slippage between the die walls and the billet. This mismatch is more pronounced in billet deformed at 100 °C than at 25 °C.

5. FEM modelling of the HPTE process

In order to explain the experimental observations above, and to calculate the strain distribution in billet at HPTE precisely, FEM simulations had been performed.

5.1. Contact friction coefficients definition

One of the most important parameter for the FEM modelling is a friction coefficient between the billet and contact surfaces of the HPTE tool (see Fig. 1c): bottom surface of the punch, top HPTE die, bottom HPTE die and top surface of the plug providing back pressure. It was discussed in the previous section that there was a slippage between the die walls and the billet. In order to choose the relevant values of the friction coefficient on all contact surfaces from the QForm Standard Lubricant Database, the experimentally obtained helical shape of the Al wires after HPTE (Fig. 6) was compared with the shape of the marker lines of the simulated samples (Fig. 3. 3D images of the billet and marker lines, used for the FEM, before (a) and after processing (b)b). In that way, values of the friction coefficients ensuring the coincidence of the HPTE tool rotations and the number of marker line loops were used for the FEM calculations, for that the friction coefficient was varied in the

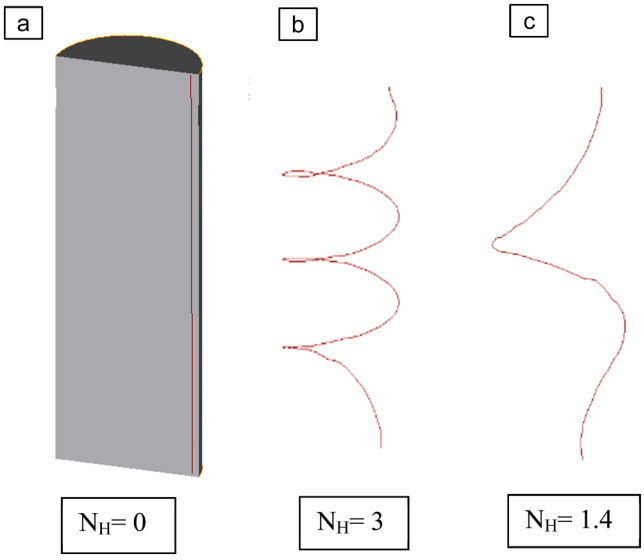

Fig. 7. FEM-simulated configurations of the marker lines after the HPTE process executed by *v*10*ω*0 (a) and *v*6*ω*1 (b, c)) regimes at deformation temperatures of 25 °C (b) and 100 °C (c).

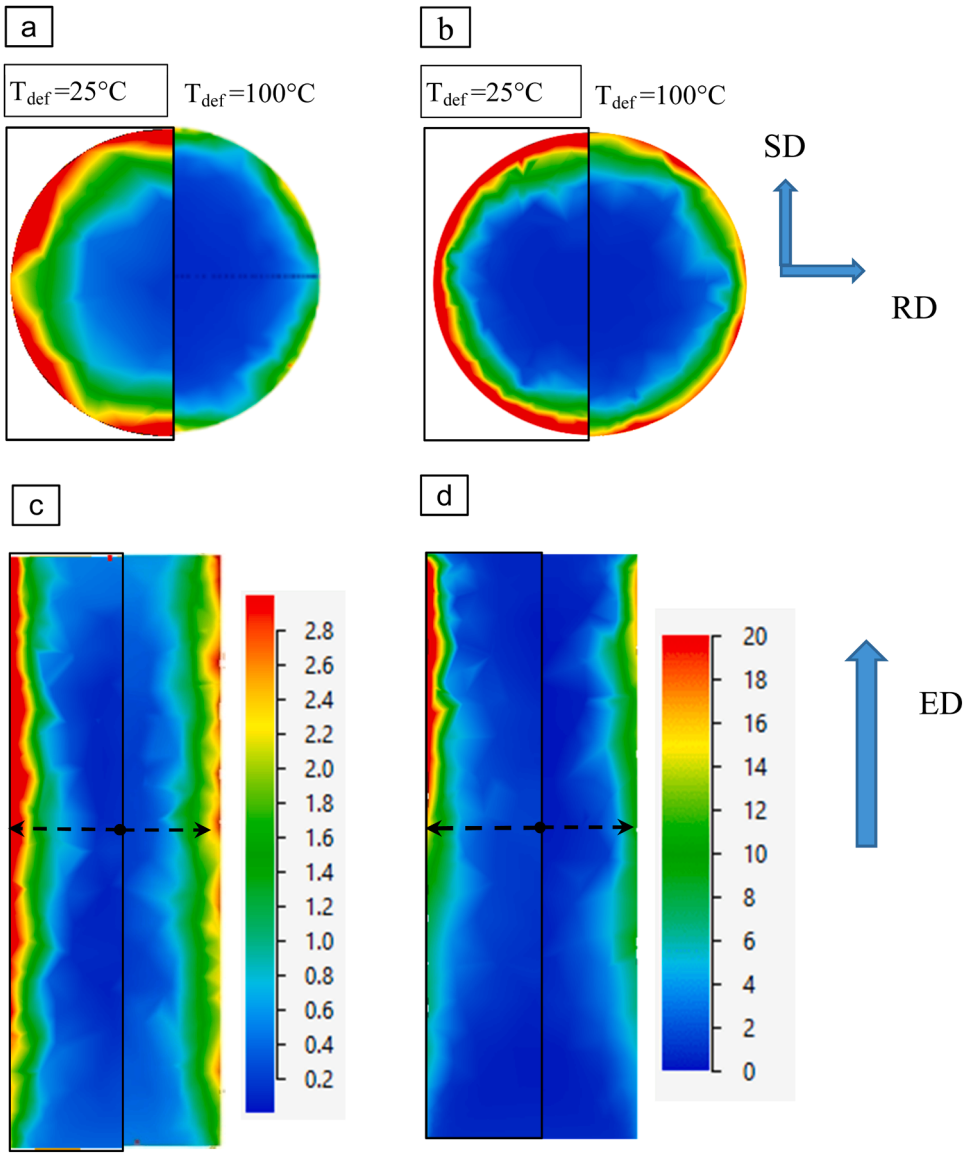

Fig. 8. Strain distribution after HPTE of copper at 100 °C (right part of a - d,) and at 25 °C (left part of a - d). HPTE regimes *v*10*ω*0 (a, c) and *v*6*ω*1 (b, d) were used for calculation and represented in transversal (a, b) and longitudinal (c, d) sections. Transversal section is taken at the half of the height of a billet.

range of 0.1–0.6. The validated values of the friction coefficients are collected in Table 3.

Note that different friction coefficients were selected for the FEM calculations of the HPTE process at 25 °C and 100 °C as the number of loops of the marker wire helixes was different at different temperatures of HPTE processing.

Here we compared the number of loops of any wire in the sample with six wires after the *v*6*w*1 regime performed at 100 °C and of the wire, placed at the same distance from the center in the sample with five wires after the same HPTE regime performed at 25 °C (it is a dark blue wire in the Fig. 6e). A big difference in the value of N_H in samples, deformed with the same HPTE regime at 25 and at 100 °C, resulted in a difference in the chosen friction coefficient values, mainly for the top die and the punch (Table 3).

5.2. *Strain analysis of the processed billets*

In the beginning of this section we demonstrate that the above discussed friction coefficients allowed to adequately reproduce the real deformation of the marker wires, described in Section 4.2, in the virtual experiment. Fig. 7 illustrates the changes in the shape of the initially straight marker line after the full HPTE processing. The *v*10*w*0 HPTE regime didn't affect the shape of the marker line, which remains straight after processing (Fig. 7a). HPTE processing with a rotation of the bottom die leads to the formation of helical shape of the marker line (Fig. 7b, c) with the number of loops equal to the number of marker wire loops N_H obtained in the respective experiments (Table 3). Note that in both cases loops were uniformly distributed almost along the whole height of the billets, except the end parts, where some spreading of helixes can be seen.

This spreading is related to the lower strain in these areas, as revealed in FEM calculated strain distributions discussed below. A similar not uniform distribution of the strain along the length of the HPTE-processed billets was also obtained in the work of Kulagin et al. (2019). It was proposed that such not uniform distribution of strain was associated with a slippage of a billet in the die during processing. Slippage is defined by friction conditions during the unstable stages of the HPTE process, namely, the initial and the final stages, when the billet is not properly fixed in the holding elements in the die.

Let us discuss the strain distributions in billets processed at various

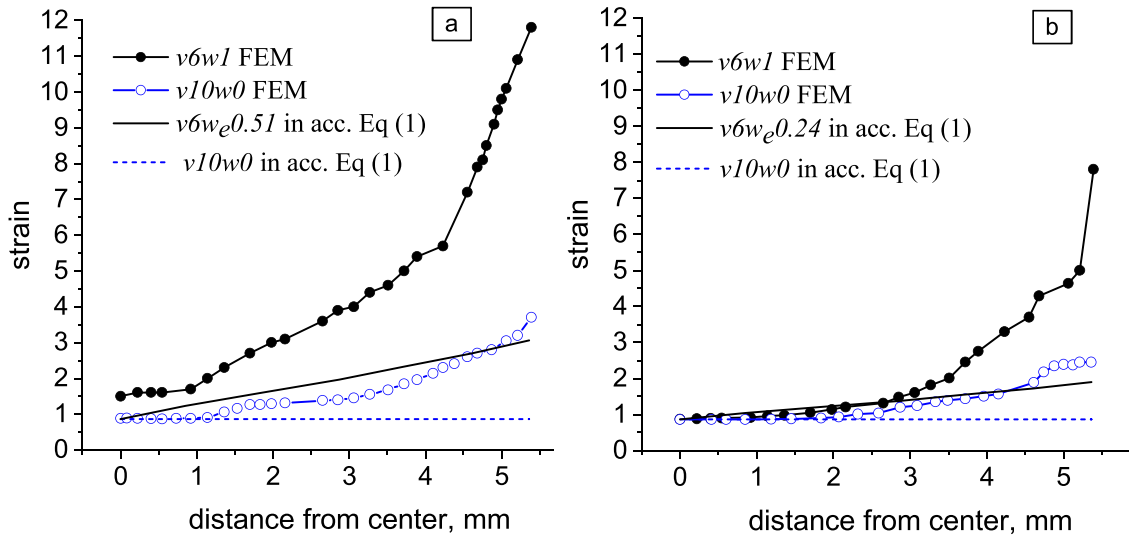

Fig. 9. Accumulated strain distribution in transversal cross section at the half of billet height, calculated by FEM and by Eq. (1): for the *v*10*ω*0 and *v*6*ω*1 HPTE regimes at 25 (a) and 100 (b)°C. For the strain estimate by Eq. (1) experimentally obtained values of rotation velocity w_e from Table 3 were used.

HPTE regimes calculated by FEM. The *v*10*w*0 HPTE regime without a rotation of the bottom die leads to the hexagon shape of the strain distribution in a transversal cross section of a billet (Fig. 8a), whereas after the *v*6*ω*1 regime (Fig. 8b) the strain distribution is smoother (ring-like).

Strain distribution maps in the transversal and longitudinal billet cross section after the *v*10*w*0 HPTE regime at room temperature have demonstrated less strain in the center and in the middle-radius area and higher strain in the edge area in comparison with these values at the same HPTE regime at 100 °C (Fig. 8a, c). Significantly higher resulting strain is provided by the HPTE processing in the *v*6*w*1 regime (Fig. 8b, d). Note that the strain values in this sample processed at room temperature are much higher, than these values achieved at 100 °C (compare left and right images in Fig. 8b, c). This difference results from the different hardening behavior of Cu at room temperature and at 100 °C (Fig. 4).

Considering strain distribution in the longitudinal section of a billet after different HPTE regimes, one can see that a gradient of strain from the center to the periphery along the RD is present over the whole height of the billets (Fig. 8c, d). In the billet after the *v*10*w*0 HPTE regime, such gradient strain distribution looks more or less uniform along the billet height (Fig. 8c). Whereas the *v*6*w*1 HPTE regime with a rotation of the bottom die provides the strongest gradient in the top part of a billet (Fig. 8b, d). The variation of deformation temperature does not change the character of the strain distribution, but leads to higher strains at a lower deformation temperature (25 °C) for all HPTE regimes (Fig. 8c, d).

In order to illustrate the strain distribution in the HPTE-processed billets clearer, we have plotted the variation of the accumulated strain from the center of the billet to its edge in the middle of its height along the dashed lines, drawn in Fig. 8c, d (Fig. 9). For comparison, in Fig. 9 we also plotted the strain distributions along the billet radius calculated according to analytic Eq. (1) using the experimental values of the rotation velocity w_e from Table 3. Note that strain distributions calculated by Eq. (1) are close to the FEM-calculated ones only for the *v*10*w*0 and *v*6*w*1 regimes at 100 °C, and for the central and middle parts of the billet (Fig. 9b).

For all other regimes or billet locations, a strong deviation between the strain distributions calculated by Equation (1) and by FEM were observed. In particular, in billets subjected to the *v*10*ω*0 and *v*6*w*1 HPTE regimes, the FEM-calculated strain grown exponentially in the close vicinity to the edge due to the surface friction (Fig. 9), in agreement with results of Nugmanov et al. (2019). Analytic equation does not predict such behavior. The main assumption in the analytical Eq. (1) is that the sections of the sample perpendicular to the extrusion axis remain flat, but in fact they are distorted, which leads to a change in the shape of the marker cross section, see e.g. (Kulakov et al., 2022) Upon that, after the *v*6*w*1 regime, the strain gradient from the center to the edge was stronger than that after the HPTE regime without rotation (from ~ 1.4 to ~ 8.0 and from ~ 0.8 to ~ 3.0, respectively) (Fig. 9). Furthermore, for the *v*6*ω*1 HPTE regime at 25 °C, FEM calculations resulted in significantly higher strain values as compared to the strains calculated from Eq. (1).

6. Conclusions

- Accumulated strain at HPTE is a sum of shear (twisting) and expansion-extrusion deformation, there is also a strong shearing due to friction and typical for the extrusion flow distortion, especially in the periphery region of the billet. The major contribution to the accumulated strain is provided by twisting of the billet in the HPTE die.
- Experimental observations of the change of the marker wires shape and FEM calculations revealed a presence of a significant slippage between the HPTE die walls and the billet. This slippage is more pronounced in billets deformed at 100 °C than at 25 °C.
- HPTE allows to obtain rather high strain values during one HPTE pass. For example, the strain values in copper billets processed via the *v*6*ω*1 regime at 25 °C vary from 1.5 in the billet center to 12 at its perifery, which is much higher than strain after one ECAP pass or one twist extrusion pass.

Declaration of Competing Interest

The authors declare the following financial interests/personal relationships which may be considered as potential competing interests: Nugmanov Dayan reports a relationship with Karlsruhe Institute of Technology North Campus that includes: employment. Ivanisenko Julia has patent #DE102013213072A1 issued to V. FEDOROV, J. IVANISENKO, B. BARETZKY, H. HAHN.

Data Availability

Data will be made available on request.

References

Baik, S.C., Estrin, Y., Hellmig, R.J., Jeong, H.-T., Brokmeier, H.G., Kime, H.S., 2003. Modeling of texture evolution in copper under equal channel angular pressing. Int. J. Mater. Res. 94 (11), 1189–1198.

Beygelzimer, Y., Orlov, D., Korshunov, A., Synkov, S., Varyukhin, V., Vedernikova, I., Reshetov, A., Synkov, A., Polyakov, L., Korotchenkova, I., 2006. Features of twist extrusion: method, structures & material properties. Solid State Phenom. 114, 69–78.

Biba, N., A. Maximov, S. Stebunov, A. Vlasov, 2012. The model for simulation of thermally, mechanically and physically coupled problems of metal forming. In: Proceedings of the 14th international conference on metal forming, Krakow, Poland.

Fedorov, V., J. Ivanisenko, B. Baretzky, H. Hahn, 2015. DE Patent: DE102013213072A1.

Grewe, H.G., Kappler, E., 1964. Über die Ermittlung der Verfestigungskurve durch den Torsionsversuch an zylindrischen Vollstäben und das Verhalten von vielkristallinem Kupfer bei sehr hoher plastischer Schubverformung. Phys. Status Solidi B 6 (2), 339–354.

Holm, E.A., Miodownik, M.A., Rollett, A.D., 2003. On abnormal subgrain growth and the origin of recrystallization nuclei. Acta Mater. 51 (9), 2701–2716.

Ivanisenko, Y., Kulagin, R., Fedorov, V., Mazilkin, A., Scherer, T., Baretzky, B., Hahn, H., 2016. High pressure torsion extrusion as a new severe plastic deformation process. Mater. Sci. Eng.: A 664, 247–256.

Kulagin, R., Latypov, M.I., Kim, H.S., Varyukhin, V., Beygelzimer, Y., 2013. Cross flow during twist extrusion: theory, experiment, and application. Metall. Mater. Trans. A 44 (7), 3211–3220.

Kulagin, R., Beygelzimer, Y., Estrin, Y., Ivanisenko, Y., Baretzky, B., Hahn, H., 2019. A mathematical model of deformation under high pressure torsion extrusion. Metals 9, 3.

Kulakov, M., Mail, M, Kulagin, R., 2022. The effect of the die rotation during extrusion on the shape of embedded markers. Materials Letters 322, 132486.

Levanov, A.N., 1997. Improvement of metal forming processes by means of useful effects of plastic friction. J. Mater. Process. Technol. 72 (2), 314–316.

Li, X., Reza-E-Rabby, M., Guzman, A., Grant, G., Mathaudhu, S., Hinton, M., Reynolds, A., 2022. Strain and strain rate in friction extrusion. J. Mater. Res. Technol. 20, 882–893.

Mizunuma, S., Iizuka, T., Mitsui, K., Okumura, H., Kohzu, M., 2010. Grain refinement of magnesium alloy AZ31 under torsion extrusion with a square-hole die. Mater. Sci. Forum 654–656, 711–714.

Nugmanov, D., Mazilkin, A., Hahn, H., Ivanisenko, Y., 2019. Structure and tensile strength of pure Cu after high pressure torsion extrusion. Metals 9, 10.

Pardis, N., Talebanpour, B., Ebrahimi, R., Zomorodian, S., 2011. Cyclic expansion-extrusion (CEE): A modified counterpart of cyclic extrusion-compression (CEC). Mater. Sci. Eng. A-Struct. Mater. Prop. Microstruct. and Processing 528 (25–26), 7537–7540.

Pippan, R., Scheriau, S., Hohenwarter, A., Hafok, M., 2008. Advantages and limitations of HPT: a review. Mater. Sci. Forum 584–586, 16–21.

Toth, L.S., Chen, C., Pougis, A., Arzaghi, M., Fundenberger, J.-J., Massion, R., Suwas, S., 2019. High pressure tube twisting for producing ultra fine grained materials: a review. Mater. Trans. 60 (7), 1177–1191.

Valiev, R.Z., Islamgaliev, R.K., Alexandrov, I.V., 2000. Bulk nanostructured materials from severe plastic deformation. Prog. Mater. Sci. 45 (2), 103–189.